

Sub-Surface Crack Propagation in Hypoid Gear

M. Guagliano, L.Vergani, M. Vimercati

Politecnico di Milano, Mechanical Engineering Dept.
Via La Masa 34, 20158 Milan (ITALY)
martino.vimercati@polimi.it

ABSTRACT. *This paper proposes a numerical approach devoted to the investigation of the sub-surface crack propagation mechanism in gear pairs having crossing axis (i.e hypoid gears). Starting from an accurate 3D description of the complex gear tooth geometry, a numerical analysis carried out by means of an advanced contact solver allows obtaining, over the entire meshing cycle, the contact pressure distribution and the displacement field in the uncracked tooth. Then, such displacements are applied as boundary conditions to a second finite element model of the cracked zone, being the aim the stress intensity factor calculation for the mode I, II, III along the crack front. At this point it is possible to examine the crack growth mechanism: the maximum shear SIF range and the maximum tensile SIF range are computed and considerations about direction of crack propagation are drawn. As application of this approach, a circular sub-surface crack in a real hypoid gear of a truck differential transmission is analysed.*

1 INTRODUCTION

Nowadays, due to the ever more severe requirements which machines have to accomplish (namely heavier loads at minimum weight), the engineers are called for a “design by analysis” process, i.e. a more refined design including very accurate simulations able to reproduce the actual working condition of the components. This approach is especially needful for applications, such as gear, bearing or rail/wheel, where two or more components are in contact. In these applications, in fact, it is fundamental to investigate the mechanisms of the damage and, starting from this knowledge, to be able to predict the component failure.

Referring to gear field, it is known [1] that the gear drive reliability is mainly influenced by the damages which can occur due to fatigue loading conditions. In particular, it is possible to distinguish two phenomena: the bending fatigue failure at the tooth root and the surface deteriorations (pitting/spalling) due to rolling contact fatigue (RCF). This latter mechanism will be the main issue of this paper; in particular the authors attention will be focused on the spalling which finds its origin in cracks placed at some distance from the surface, usually in correspondence of an internal material defect sited near the position of maximum shear stress.

An accurate literature survey makes clear that many papers about gear RCF damage have been proposed. Blake et al. developed a pitting life model based on fracture mechanics in order to estimate service lives and failure probabilities in spur gear [2]; Glodez et al. presented several models for simulation of the surface fatigue process in the contact area, allowing a proper determination of the spur gear pitting/spalling resistance [3]; Flodin et al. proposed models for wear prediction in helical gears [4]; Ding et al. found in the ligament collapse the mechanism for spalling formation in spur gear [5]; Guagliano et al. described a Weight Function based approach to predict spur gear spalling [6]; Aslantas et al. developed a study of spur gear pitting formation and life prediction [7]. As evident, the gears considered in all of these works are cylindrical, that is, they are characterized by simple tooth geometry and it is possible to handle

them using 2D schematisation. On the contrary, RCF in gear pairs having crossing or intersecting axes - such as spiral or hypoid gear which are widely employed in aerospace or automotive field - have not yet significantly investigated; nowadays the only way to handle this subject is to refer to the International Standards [8] which are very conservative and do not accomplish the previously mentioned “design by analysis”. The cause of this lack of knowledge is reasonably related to the fact that it is a really tough task to reproduce the complicated tooth geometry and to simulate the intricate meshing condition which typically occurs for these categories of gear.

Aim of this paper is just to propose a numerical tool able to investigate the working condition of internal cracks in spiral or hypoid gears. Starting from a previously developed study which is originally aimed to analyse cracked railway wheel [9], the approach is based on the following steps (see Fig. 1). Firstly, a 3D contact/stress analysis, which is carried out by means of an advanced numerical solver [10], allows to calculate very precisely the contact pressure distribution over the un-cracked teeth during the whole meshing cycle [11]; then, this non-Hertzian pressure distribution is provided as loading condition for the calculation, according to the Boussinesq theory, of the displacement field in the un-cracked tooth which is properly reduced to a half-space; finally, the calculated displacement components are applied as boundary conditions to a finite element model of the zone surrounding the crack allowing the computation of the stress intensity factors along the crack front. This approach allows obtaining easily and with limited calculation time results concerning different values of the input parameters (mainly position, dimensions and shape of the crack) over a complete loading cycle.

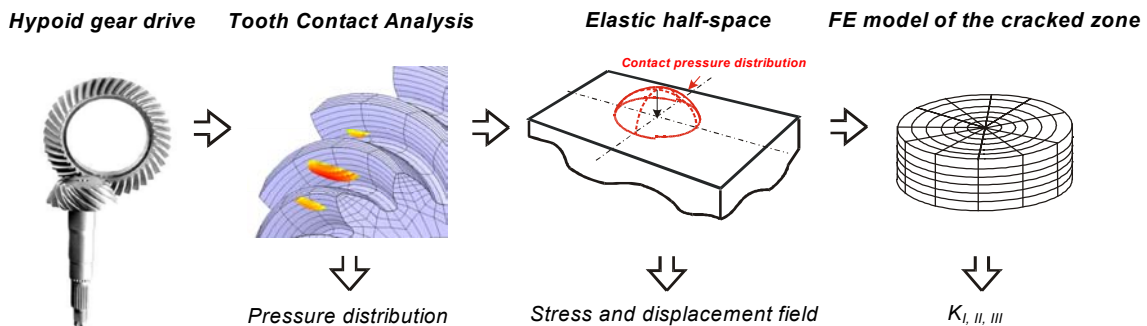


Figure 1. Approach for determining the stress intensity factors of internal cracks in hypoid gears.

Once the SIF along the crack front is known, it is possible to deal with the crack growth mechanism; in particular, this paper is aimed to investigate the direction of crack propagation. Criteria able to accomplish this task are discussed in the literature: the maximum tangential stress [12] or the strain energy density [13] are widely used to predict crack propagation direction under mixed mode (K_I e K_{II}) static condition; Kaneta et al. studied the propagation direction of a subsurface crack under cyclic loads assuming that shear and tensile crack growth occurs, respectively, in the plane of maximum shear or tensile SIF, and reported that, in case of pure rolling (frictionless condition) the crack have the tendency to extend in shear mode along the original crack plane while, when the surface traction are large enough, tensile crack growth can take place and the crack tip at the trailing side reaches the surface [14]; the approach of Komvopoulos et al. [15] is similar to [14] but it examined the subsurface crack growth behaviour using the ranges of the maximum shear and tensile SIF instead of the maximum shear or tensile SIF tout-court.

The present paper describes the results obtained for the hypoid gearset belonging to a real

differential truck transmission: the trend of stress intensity factor for the Mode I, II and III, which are obtained by means of the aforementioned procedure, allows the evaluation of the maximum shear and tensile SIF ranges and, accordingly to [15], the understanding of crack growth direction.

2. PROCEDURE FOR SIFs COMPUTATION

The present approach consists in three main steps (see Fig. 1): computation of the contact pressure distribution in the un-cracked tooth, evaluation of the displacement field under the tooth surface and calculation of the SIFs along the crack front. The reliability of the method has been previously verified [9] by comparing it with models from literature; in particular, the results showed a difference less than 10% with respect of the data collected in [14].

2.1 Determination of the contact pressure distribution

The knowledge of the contact pressure distribution over the tooth active flank requires a gear contact analysis [16]. In order to reliably accomplish this task, it is of great importance to describe very accurately the geometry of the mating surfaces. In this paper an articulate algorithm based on the numerical simulation of the gear cutting process [11] allowed to obtain very precisely the mathematical representation of hypoid gear tooth surfaces. Then, the so computed gear tooth surfaces have been employed as input for an advanced contact solver which combines a semi-analytical surface integral theory (for solving the contact problem) and the traditional finite element method (for computation of gross deflections associated with tooth bending) [10]. This approach makes possible to carry out very accurate contact analysis and stress calculation employing a relative coarse mesh; in particular, unlike the usual solvers based only on FEM, a locally refined mesh around the contact region is not required. Figure 2 reports the representation of the pinion meshing with the driven gear member and the contact pressure 3D plots computed in one meshing instant [11]. It is evident that the load is shared between more than one tooth pair and that the pressure distribution shows a characteristic sharp and oblong shape which hardly could be predicted by the Hertz theory which, instead, is usually adopted in spur gear.

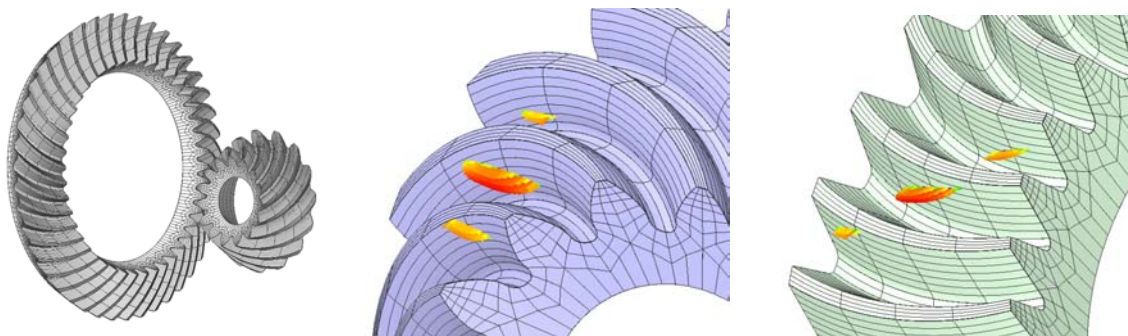


Figure 2. Geometric representation and contact pressure distribution for the studied hypoid gear.

2.2 Determination of the tooth sub-surface displacement field

With the aim to calculate the displacement field due the contact pressure distribution, the tooth is schematized as a half-space. This assumption can be considered realistic for the tooth of the driven member. In fact, unlike the pinion, the cutting process usually adopted for manufacturing this member [17] produces a simpler tooth geometry allowing to neglect the curvature along the tooth profile. For these reasons, the following discussion is referred to the gear member and the

loading condition is reduced to a pressure distribution applied to the free plane of a half-space. Figure 3 shows from different points of view the contact pressure computed in one meshing instant applied to the two dimensions geometric development of the gear tooth convex surface; x-axis and y-axis are the measures of the curvilinear coordinate respectively along the face width and along the profile of the tooth.

In order to obtain the displacement field under the tooth surface, that pressure distribution is firstly schematised as a set of finite number of point forces normal to the free surface of the half-space; then, using the Boussinesq theory [18-19], the displacement components induced by each of those point loadings are analytically computed; by adding the contribute of each point loading, the displacements everywhere in the half-space is known.

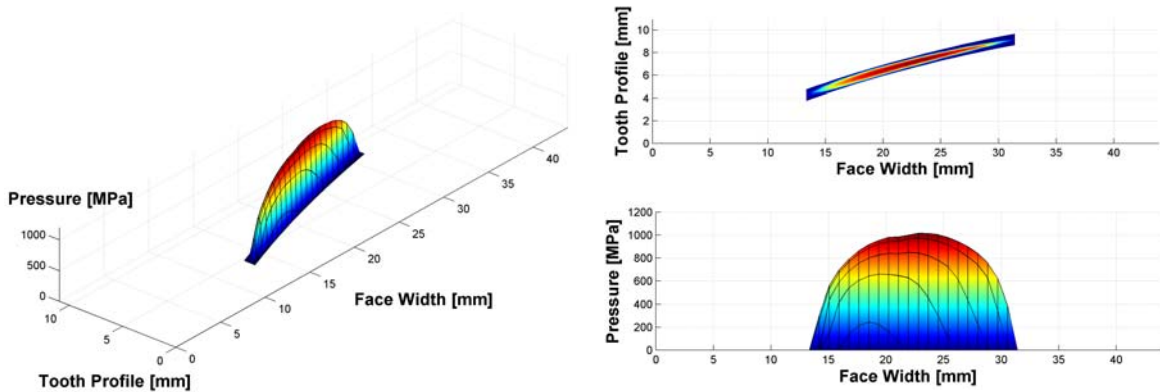


Figure 3. Some viewing points of the pressure distribution on the gear tooth convex surface.

2.3 Determination of the SIFs

With the aim to evaluate the SIF for Mode I, II and III along the crack front, the displacements obtained by the previous step are applied as boundary condition to a 3D finite element model of the zone surrounding the crack with radius equal to a (Fig.e 4). Brick elements with 20 nodes and second order shape functions were used. Special elements were also used to simulate the contact between the crack faces, avoiding their overlapping. The friction between the crack faces can be included in the model. This model allows a very refined mesh near the crack front, where the $\frac{1}{4}$ point technique was used to better simulate the stress singularity according to LEFM.

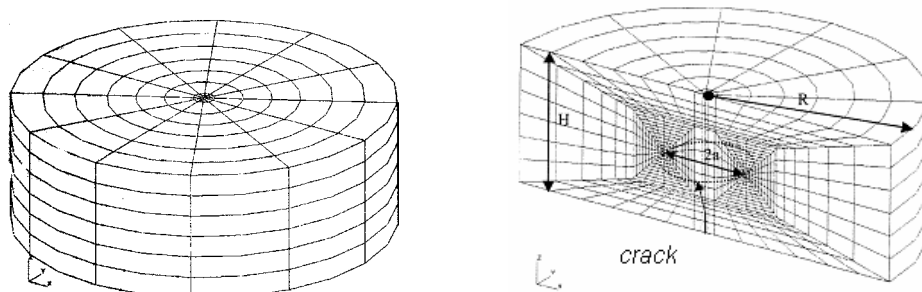


Figure 4. Finite element model of the zone around the crack.

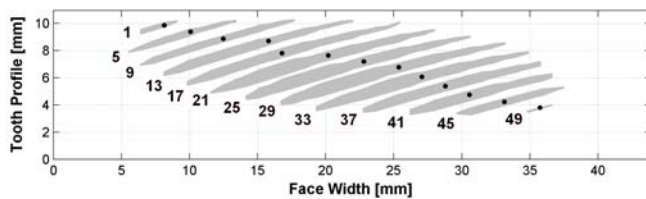
3 RESULTS AND DISCUSSION

The proposed approach has been employed to study the crack growth mechanism in a real hypoid gear drive which belongs to a truck differential system. The basic geometric data of the gear pair are reported in Table 1. The material is surface hardened 21NiCrMo4 steel (UTS = 1650 MPa, YS = 1100 MPa). The friction between the mating surfaces is low ($\mu = 0.04 - 0.06$) allowing to simulate the contact as frictionless.

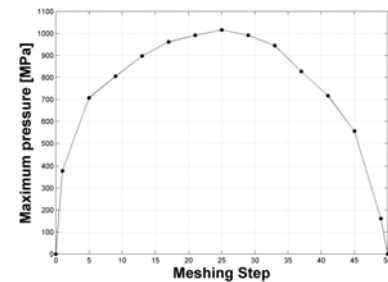
In order to carry out the contact analysis, a value of input torque equal to 250 Nm is considered and the whole meshing cycle is divided and analysed in 50 steps (more detail about this contact analysis are described in [11]). Referring to the convex side of one gear tooth, in Figure 5.a the complete loading history is reported (for sake of clarity, the contact pattern of only 13 instants extracted from the previously mentioned 50 analysis cases are plotted); for each pattern the point of maximum pressure is highlighted by a black point. Figure 5.b reports the trend of maximum pressure value versus the meshing step. These graphs make clear that in the 25th step the highest pressure value (1016 MPa) is reached; it is also evident that the pressure pattern travels in a complicated way over the tooth flank and that the contact pressure distribution related to a particular meshing instant is quite different from the others.

Table 1. Basic geometric parameters of the analyzed hypoid gear drive.

Parameter		Pinion	Gear
Module	[1/mm]	5.11	
Shaft Angle	[°]	90	
Offset	[mm]	25	
Number of Teeth		15	44
Mean Spiral Angle	[°]	43.00	28.90
Hand of Spiral		Left	Right
Face Width	[mm]	41.43	38.00
Outer Cone Distance	[mm]	106.40	126.10
Pitch Angle	[°]	26.88	62.41
Addendum	[mm]	5.09	2.96
Dedendum	[mm]	3.91	6.04



a – Whole contact pattern history.

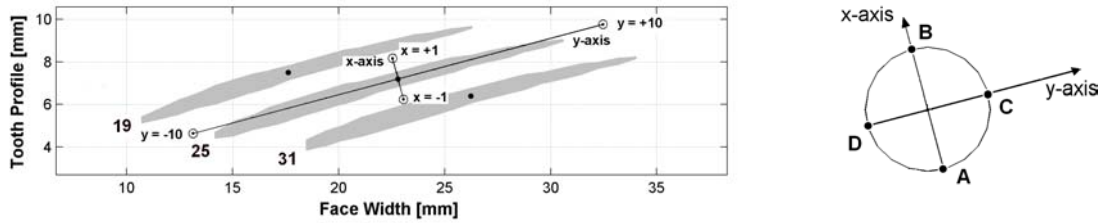


b – Maximum pressure vs meshing instant.

Figure 5. Details of the contact pressure distribution computed during the whole meshing.

Once the loading history is known, the proposed approach allows calculating the SIFs for cracks having any shape, dimension and position during the whole meshing cycle. In this paper a circular crack with radius a equal to 0.2 mm is considered. With the aim to study the most critical tooth zone, the attention of the authors has been focused on the region just under the contact pressure computed in the 25th meshing step. Considering this loading case, in the point of maximum pressure a reference frame having the axes parallel to the axes of the pseudo

contact ellipse, is placed (Fig. 6.a). As discussed also in a previous study [20], referring to the crack centre, the crack positions reported in Table 2 are analysed; that is, the crack has been moved along the x-axis and the y-axis laying on a plane parallel to the free surface to a depth equal to 0.25 mm (corresponding to the position where the shear stress is maximum). In Figure 6.a, the crack in the four extreme positions (corresponding to an eccentricity on x-axis equal to ± 1.0 mm and on y-axis equal to ± 10 mm) is reported. Figure 6.a also shows that all the crack positions have been analyzed considering the meshing step from the 19th through 31st; in fact, it has been verified that, for such crack positions, all the remaining loading steps have no significant influence on the SIF value. It is finally convenient to define four points on the crack front (Fig 6.b): points A and B are aligned with the x-axis; points C and D are aligned with the y-axis. These points are the ones considered for the stress intensity factor calculation. Making a conservative assumption, contact between crack faces is simulated as frictionless.



a – Crack position on the tooth surface.

b – Calculation points along the front.

Figure 6. Schematization used in the analysis and definition of the main parameters.

Table 2. Positions of the crack considered in the analysis.

Crack Center Coordinate					Crack Center Coordinate		
x [mm]	y [mm]	z [mm]		x [mm]	y [mm]	z [mm]	
x-1.0	-1.00	0.00	0.25	y-10	0.00	-10.00	0.25
x-0.8	-0.80	0.00	0.25	y-8	0.00	-8.00	0.25
x-0.6	-0.60	0.00	0.25	y-6	0.00	-6.00	0.25
x-0.4	-0.40	0.00	0.25	y-4	0.00	-4.00	0.25
x-0.2	-0.20	0.00	0.25	y-2	0.00	-2.00	0.25
x 0.0	0.00	0.00	0.25	y 0	0.00	0.00	0.25
x+0.2	0.20	0.00	0.25	y+2	0.00	2.00	0.25
x+0.4	0.40	0.00	0.25	y+4	0.00	4.00	0.25
x+0.6	0.60	0.00	0.25	y+6	0.00	6.00	0.25
x+0.8	0.80	0.00	0.25	y+8	0.00	8.00	0.25
x+1.0	1.00	0.00	0.25	y+10	0.00	10.00	0.25

3.1 Stress intensity factors

In this paper, being the aim to investigate the crack growth mechanisms, just a brief overview about that SIF results is provided; a more detailed description about this issue is kept in [20].

Due to the fact that the contact between the mating surfaces is simulated as frictionless, no surface traction loads are present and consequently the SIF for mode I is always null.

On the other hand, K_{II} values shown significant fluctuation when the load position is varying: Figure 7.a reports, referring to point A, the trend of K_{II} for the crack in position ($x = 0$; $y = 0$) and Figure 7.b summarizes the trend of ΔK_{II} versus the crack positions along the x-axis in the same point. It is simple to figure out that the value of ΔK_{II} remains quite stable around 7 MPa \sqrt{m} . The trends of K_{II} in point B has been verified to be very similar to the ones reported for point A. Value of ΔK for mode III in points A and B has been found to be always lower than 0.2

MPa√m and consequently it can be neglected.

Regarding K_{III} in points C, the trends are very similar to the ones obtained for K_{II} in point A (Fig. 7.c and 7.d); the main difference is that, now, the ΔK_{III} value is lower (~ 4.5 MPa√m). K_{II} values for point C are negligible (< 0.3 MPa√m). A similar discussion can be drawn for point D.

All these results allow to affirm that moving the crack along x-axis does not affect significantly the criticality of the crack itself. This evidence is reasonable due to the fact that, although the cracks have a different position with respect to the contact pressure history, all the cracks are subjected to a similar loading history.

Different results have been obtained analyzing the cracks placed along the y-axis: as the crack is coming closer to the origin of the reference frame (Fig. 8.a), ΔK_{II} increases, achieving the maximum value just in the point of maximum pressure. Point B can be handled in analogous way. Value of ΔK for mode III in points A and B is always lower than 0.5 MPa√m and consequently also in this case it can be neglected. Referring to K_{III} in points C and D, it is possible to make similar discussion (Fig. 8.b); just the maximum ΔK_{III} is slower (~ 5 MPa√m). Thus, the analysis along y-axis confirms that the most critical region is located near to the most loaded zone of the tooth.

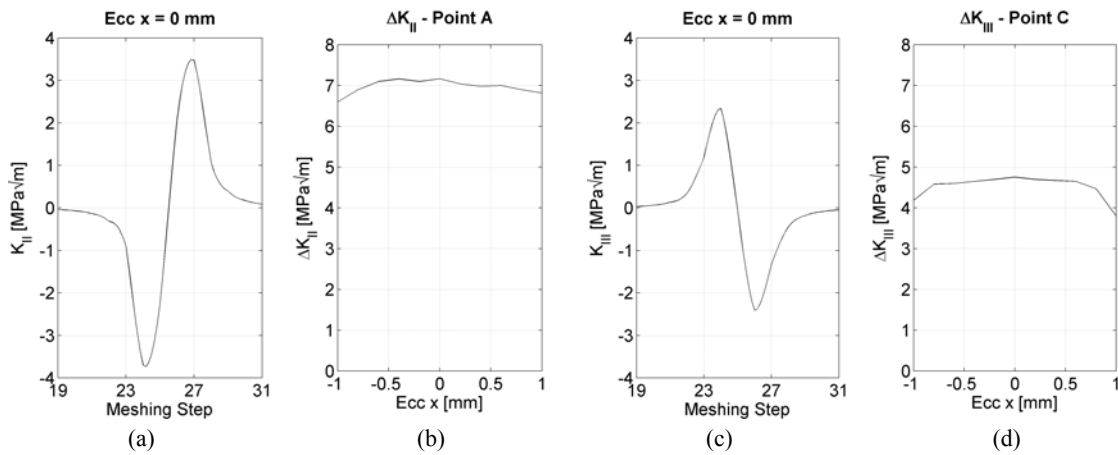


Figure 7. Stress Intensity Factor trends for Mode II and III in point A and C for cracks along x-axis.

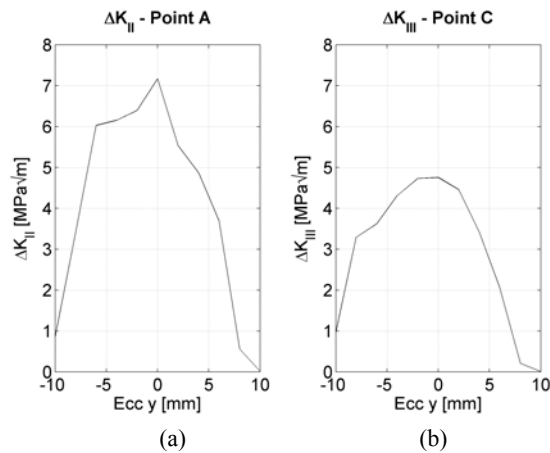


Figure 8. SIF trends for Mode II and III in point A and C for cracks along Y-axis.

3.2 Crack growth direction

According to the results showed in the previous section, the attention of the authors has been focused on the crack which is located just under the worst loading condition (i.e. $x = y = 0$ mm and $z = 0.25$ mm). In particular, points A and B, where the maximum K_{II} fluctuations have been detected, are considered; as previously shown, in these locations K_{III} is nearly null.

Referring to that crack in the plane x-z (Figure 9), the stress in the tips vicinity under mixed mode I and II can be described as [12]:

$$\sigma_r = \frac{1}{\sqrt{2\pi r}} \cos \frac{\theta}{2} \left[K_I \left(1 + \sin^2 \frac{\theta}{2} \right) + \frac{3}{2} K_{II} \sin \theta - 2K_{II} \tan \frac{\theta}{2} \right] \quad (1)$$

$$\sigma_\theta = \frac{1}{\sqrt{2\pi r}} \cos \frac{\theta}{2} \left[K_I \cos^2 \frac{\theta}{2} - \frac{3}{2} K_{II} \sin \theta \right] \quad (2)$$

$$\tau_{r\theta} = \frac{1}{2\sqrt{2\pi r}} \cos \frac{\theta}{2} \left[K_I \sin \theta + K_{II} (3 \cos \theta - 1) \right] \quad (3)$$

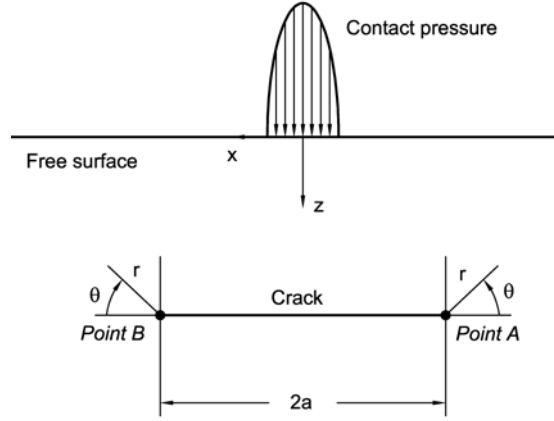


Figure 9. Crack in plane x-z and definition of the coordinate system for the computation of the stress at the crack tip.

The tensile and shear SIF (K_σ and K_τ) can be defined as follows:

$$K_\sigma(\theta) = \sigma_\theta \sqrt{2\pi r} = \cos \frac{\theta}{2} \left[K_I \cos^2 \frac{\theta}{2} - \frac{3}{2} K_{II} \sin \theta \right] \quad (4)$$

$$K_\tau(\theta) = \tau_{r\theta} \sqrt{2\pi r} = \frac{1}{2} \cos \frac{\theta}{2} \left[K_I \sin \theta + K_{II} (3 \cos \theta - 1) \right] \quad (5)$$

It is evident that, for a given value of θ (i.e. $\theta = \bar{\theta}$), K_σ and K_τ are functions of the K_I and K_{II} and consequently they fluctuate according to the load position. In order to find the direction propagation of the crack, it is useful to compute the tensile and shear range for $\theta = \bar{\theta}$:

$$\Delta K_{\sigma|\theta=\bar{\theta}} = K_{\sigma,\max|\theta=\bar{\theta}} - K_{\sigma,\min|\theta=\bar{\theta}} \quad (6)$$

$$\Delta K_{\tau|\theta=\bar{\theta}} = K_{\tau,\max|\theta=\bar{\theta}} - K_{\tau,\min|\theta=\bar{\theta}} \quad (7)$$

Doing so for all the value of θ ($-180 \leq \theta \leq 180$), it is possible to find the trend of ΔK_{σ} and ΔK_{τ} as function of the angle θ . Figure 10 shows, for point A, the trend of the tensile and shear range, which are computed by using the SIF obtained in the previous section. Trends for point B are not reported because they are very similar to the ones calculated for the point A; in fact these points are subjected to a very similar loading history as well.

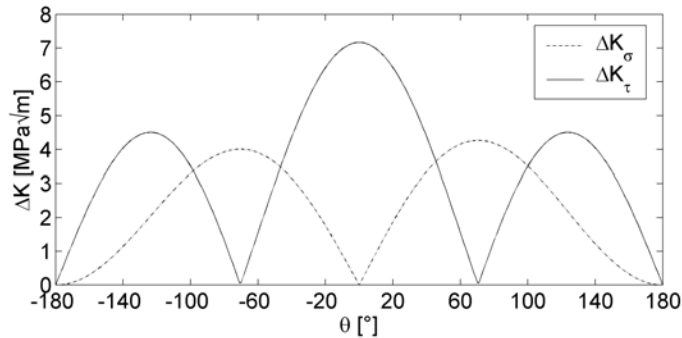


Figure 10. Trend of the tensile and shear ranges vs crack propagation direction in point A.

It is possible to note that the maximum value of ΔK_{τ} occur at $\theta = 0^{\circ}$, while those of ΔK_{σ} are at $\theta = \pm 70.5^{\circ}$; due to the fact the shear mechanism is dominant (i.e. $\max(\Delta K_{\tau}) > \max(\Delta K_{\sigma})$), it is reasonable to affirm that the subsurface crack show a propensity for in-plan growth (Figure 11.a). On the other hand, when the tensile mechanism is dominant (i.e. $\max(\Delta K_{\sigma}) > \max(\Delta K_{\tau})$) a transition from shear to tensile mode crack growth (namely the crack propagate for $\theta = \pm 70.5^{\circ}$) may occur; as stated in [15], this could be the case of high-friction surfaces ($\mu > 0.25$) and long cracks (especially when they are very near to the free-surface). In such conditions, the left tip propagates toward the surface ($\theta = +70.5^{\circ}$) and the right one downward into the half space $\theta = -70.5^{\circ}$).

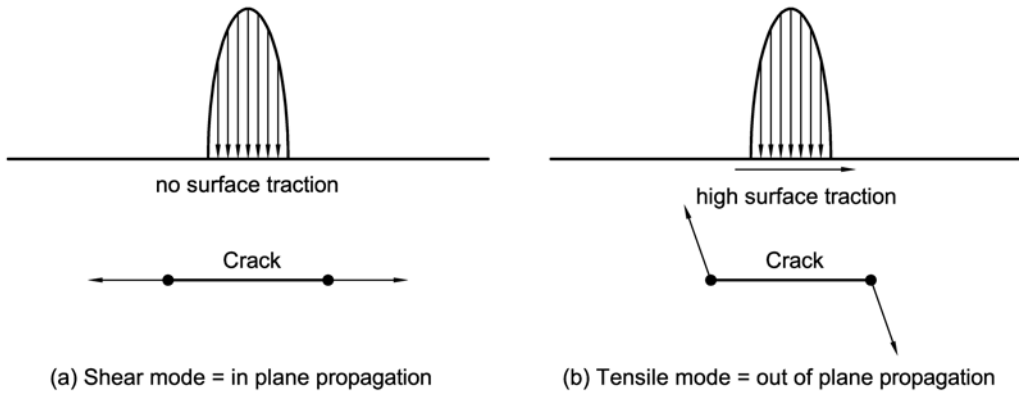


Figure 11. Possible mechanisms of crack growth.

CONCLUSION

In this paper a first attempt to study the crack growth mechanism for sub-surface cracks found in spiral and hypoid gear teeth has been proposed. The computational approach have been firstly described: the contact pressure in the un-cracked teeth are obtained by an advanced contact solver, then the displacements field due to that pressure is applied as boundary conditions to a

finite element model of the cracked zone, being the aim the stress intensity factors calculation for the mode I, II, III along the crack front. This data allowed the authors to investigate the crack growth mechanism; in particular the attention has been focused on the direction of crack propagation by means of the evaluation of the maximum shear and tensile SIF range.

As application of this procedure, a circular sub-surface crack sited in the tooth of a real hypoid gear drive which belongs to a truck differential system is considered. After schematizing the complex loading history as several pseudo elliptical contact pressure distributions, the SIFs for mode I, II and III have been computed at the crack tips. Due to the fact that the contact between the mating surface has been schematized as frictionless, in all the analyzed cases the stress intensity factor for mode I was null, while remarkable values of K_{II} and K_{III} have been obtained; in detail, it has been noted that the maximum ΔK_{II} values are reached in correspondence of the center of the pseudo ellipse corresponding to the heaviest loading step. For the crack in this location consideration about the direction of crack propagation have been finally drawn: it has been found that the shear mechanism is dominant with respect to the tensile one. This evidence induces to believe that the subsurface crack show a propensity for in-plan growth. As found in the literature [15], the tensile mechanism becomes dominant when high surface traction (namely high friction or very long cracks) is present; in this case out of plan propagation can take place.

REFERENCES

1. Dudley D. (1962) *Dudley's Gear Handbook*, McGraw-Hill, New York.
2. Blake J.W., Cheng H.S. (1991) *ASME J. Tribol. Trans.* **113** 712-718.
3. Glodez S., Flaker J., Ren Z. (1997) *Fatigue Fract. Eng. Mater. Struct.* **20**, 71-83.
4. Flodin A., Andersson S. (2001) *Wear*, **249**, 285-292.
5. Ding Y., Rieger, NF. (2003) *Wear* **254**, 1307-1317.
6. Guagliano M., Piazza A., Vergani L. (2003) *Proceedings of ASME DETC 2003*, Chicago.
7. Aslantas K., Tasgetiren S., (2004) *Wear* **257**, 1167-1175
8. ANSI/AGMA Standard 2003-B97.
9. Guagliano M., Vergani L. (2005) *Eng. Fract. Mech.* **72**, 255-269.
10. Vijayakar S.M. (1991) *Int J Numer Methods Eng* **31**, 525-545.
11. Vimercati M., Piazza A. (2005) *Proceedings of AGMA Fall Technical Meeting 2005*, Detroit
12. Erdogan F., Sih G.C. (1963) *Eng. Fract. Mech.* **85** 519-527
13. Sih G.C. (1974) *Int. J. Fract.* **10** 305-321.
14. Kaneta M., Murakami Y., Okazaki T. (1986) *ASME J. Trib.* **108**, 134-139.
15. Komvopoulos K., Cho S.-S. (1997) *Wear*, **209**, 177-183.
16. Litvin F.L. (1994) *Gear Geometry and Applied Theory*, Prentice Hall, Englewood Cliffs.
17. Stadtfeld, H.J. (2000) *Advanced Bevel Gear Technology*. The Gleason Works, Rochester.
18. Johnson K.L. (1985) *Contact Mechanics*, Cambridge University Press, London.
19. Timoshenko S.P., Goodier J.N. (1988) *Theory of Elasticity*, McGraw-Hill, New York.
20. Guagliano M., Piazza A., Vergani L., M. Vimercati, (2006) *Proceedings of 16th European Conference of Fracture*, July 3-7, 2006, Alexandroupolis.